Electronic Supplementary Information for

Heteroatom Oxidation Controls Singlet-Triplet Energy Splitting in Singlet Fission Buildings Blocks

J. Terence Blaskovits[†], Maria Fumanal[†], Sergi Vela[†], Yuri Cho[†], and Clémence Corminboeuf[†*]

[†] *Laboratory for Computational Molecular Design (LCMD), Institute of Chemical Sciences and Engineering (ISIC), École Polytechnique Fédérale de Lausanne (EPFL), CH-1015 Lausanne, Switzerland.*

E-mail: clemence.corminboeuf@epfl.ch

S1. Computational details and database

All geometries were optimized using density functional theory (DFT) at the ωB97X-D/6-31G* level with the Gaussian09 package (Revision D.01).[1] Vertical and adiabatic excitations were computed using time-dependent density functional theory (TD-DFT) within the Tamm-Dancoff approximation (TDA) to correct for triplet instabilities.[2] Full details for method benchmarking are given in previous work[3], which shows that the key excited state descriptors (ΔE_{ST}, $\Omega_{D \to A}^{S1}$ and $\Omega_{A \to A}^{T1}$) of extended conjugated chains can be approximated using vertical computations on dimers, as was done in the present study. Solvation was also shown to have little effect on the quantification of these descriptors.[3] The character of the excited states was evaluated using the charge transfer numbers ($\Omega_{i \to j}^{E}$) gathered from the transition density matrices of a given excited state E, which express the accumulation of hole and electron density on molecular fragments i and j, respectively.[4] These values are obtained by parsing the Gaussian output files with cclib[5] and using TheoDORE (version 1.7.2)[6,7] to compute the quantity of hole and electron density accumulated on the donor and acceptor fragments of the dimer. Projected density of states were generated using GaussSum, as implemented in cclib.[5] Nucleus-independent chemical shifts[8] were evaluated using the out-of-plane component of the magnetic shielding tensor at 1 Å above the centroid of each ring at the B3LYP/6-31G*[9,10] level using the gauge-independent atomic orbital (GIAO) method.[11,12] The compound geometries were optimized in the ground state at the ωB97X-D/6-31G* level of theory. As in our previous work[3], algebraic diagrammatic construction through second order (ADC(2))[13,14], was used as a reference method as implemented in the Turbomole package (version 7.2),[15] as was coupled cluster to second order (CC(2)).[16,17] The TZVP basis set was used for both methods. Monomer and dimer data are available in a Materials Cloud repository (DOI: 10.24435/materialscloud:m1-dg).
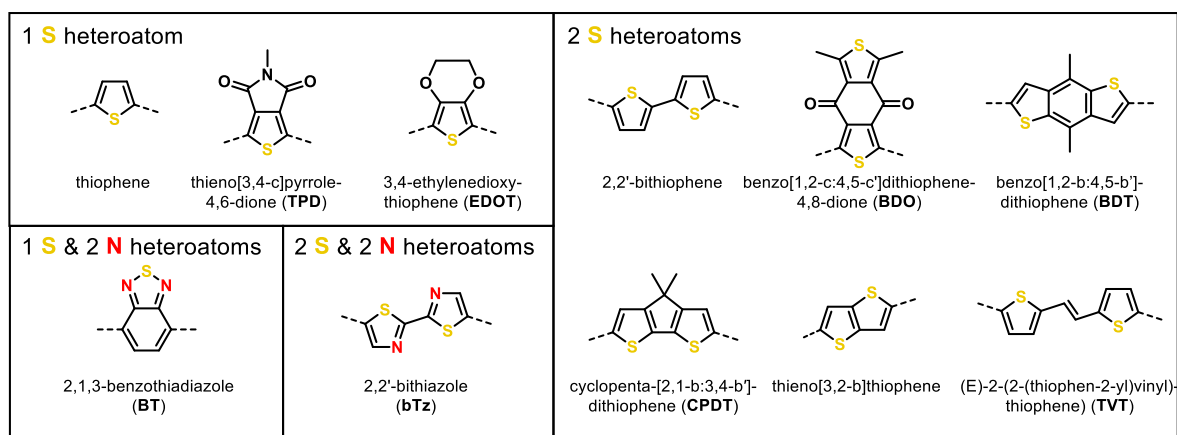

Figure S1: Dataset of building blocks studied in this work, including technical names and abbreviations. The dotted lines indicate the positions which are usually involved in coupling with adjacent units.
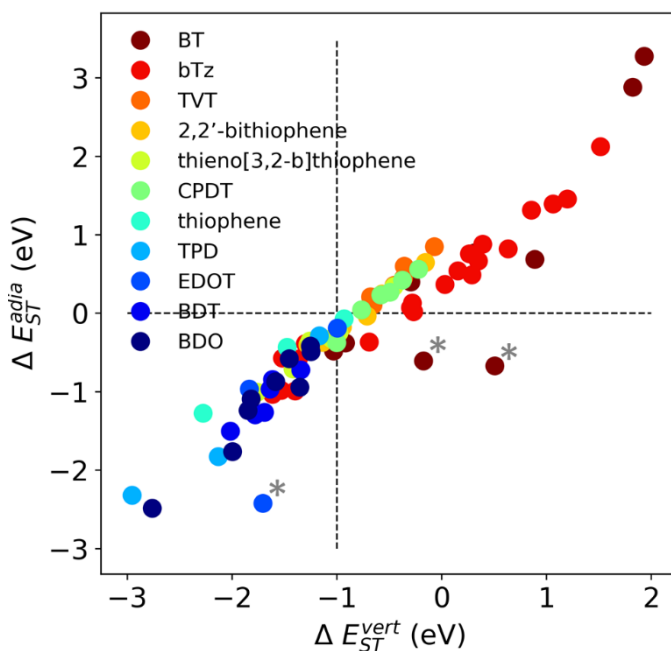
Figure S2: Comparison of the adiabatic (*y-axis*) and vertical (*x-axis*) singlet-triplet splitting for all oxidized and non-oxidized units, colored by the nature of the unit. Dotted lines serve as a visual guide for the adiabatic ($\Delta E_{ST}^{Adiab} \geq 0\ eV$) and vertical ($\Delta E_{ST}^{vert} \geq -1\ eV$) energetic criterion cutoffs. The three outlying compounds marked with asterisks exhibit ring opening upon relaxation on the S_1 energy surface, leading to spuriously low ΔE_{ST}^{adia} energies.

S2. Excited states of oxidized building block

The following plots summarize the vertical and adiabatic S_1, T_1 and ΔE_{ST} energies for all building blocks and their oxidized derivatives. Chemical structures are shown beneath each plot. The overall effect of a given oxidation pattern on S_1, T_1 and ΔE_{ST} across all building blocks is summarized in **Figure 1**. This is evaluated as the value of given property for a compound with the oxidation pattern in question with respect to a reference compound not oxidized in that position, regardless of the oxidation of other atoms, provided that they are the same in both compounds. Averages and standard deviations for the effect of each modification on are given in **Table S1**.

Table S1: Summary of the effect of a given substitution across all compounds in the dataset on adiabatic (*above*) and vertical (*below*) excited state energies (average ± σ, in eV).

Modification	ΔS_1^{adia}	ΔT_1^{adia}	$\Delta\Delta E_{ST}^{adia}$
S-oxidation	-0.74 ± 0.64	-0.43 ± 0.31	0.11 ± 0.60
S,S-oxidation	-0.41 ± 0.49	-0.51 ± 0.35	0.62 ± 0.67
N-oxidation	-0.19 ± 0.61	-0.61 ± 0.27	1.03 ± 0.80

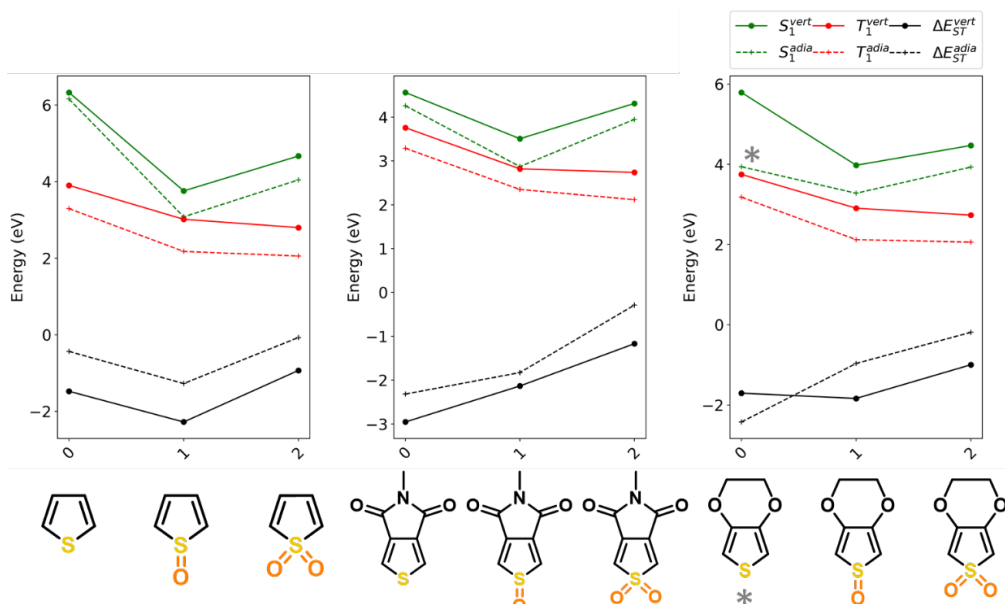| Modification	ΔS_1^{vert}	ΔT_1^{vert}	$\Delta\Delta E_{ST}^{vert}$
S-oxidation	-0.68 ± 0.58	-0.37 ± 0.24	0.07 ± 0.40
S,S-oxidation	-0.47 ± 0.40	-0.47 ± 0.28	0.46 ± 0.41
N-oxidation	-0.17 ± 0.40	-0.64 ± 0.18	1.11 ± 0.46

Figure S3: Vertical (solid lines) and adiabatic (dotted lines) singlet excitations (*green*), triplet excitations (*red*), and singlet-triplet splitting energies (*black*) of monomers containing one sulfur heteroatom (thiophene: *left*, thienopyrroledione (TPD): *center*, 3,4-ethylenedioxythiophene (EDOT): *right*) and their oxidized derivatives. The compound marked with an asterisk exhibits ring opening upon relaxation on the S_1 energy surface, leading to uncharacteristically low S_1^{adia} (and consequently low ΔE_{ST}^{adia}) energies.
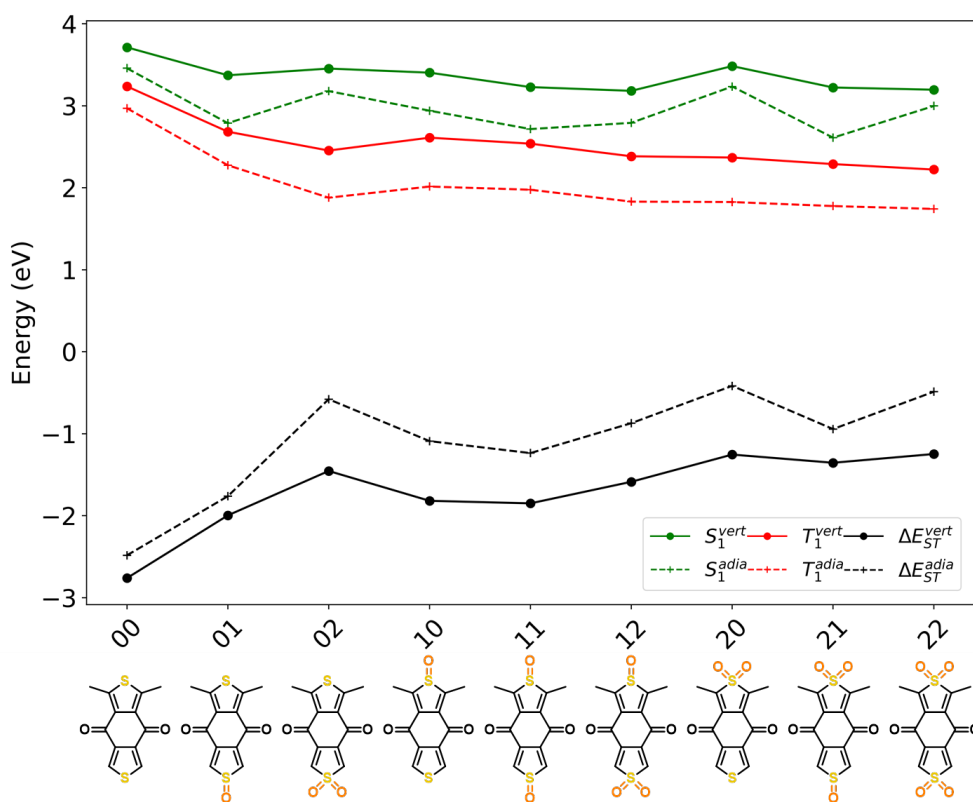
Figure S4: Vertical (solid lines) and adiabatic (dotted lines) singlet excitations (*green*), triplet excitations (*red*), and singlet-triplet splitting energies (*black*) of benzo[1,2-c:4,5-c']dithiophene-4,8-dione (BDO) and its oxidized derivatives.
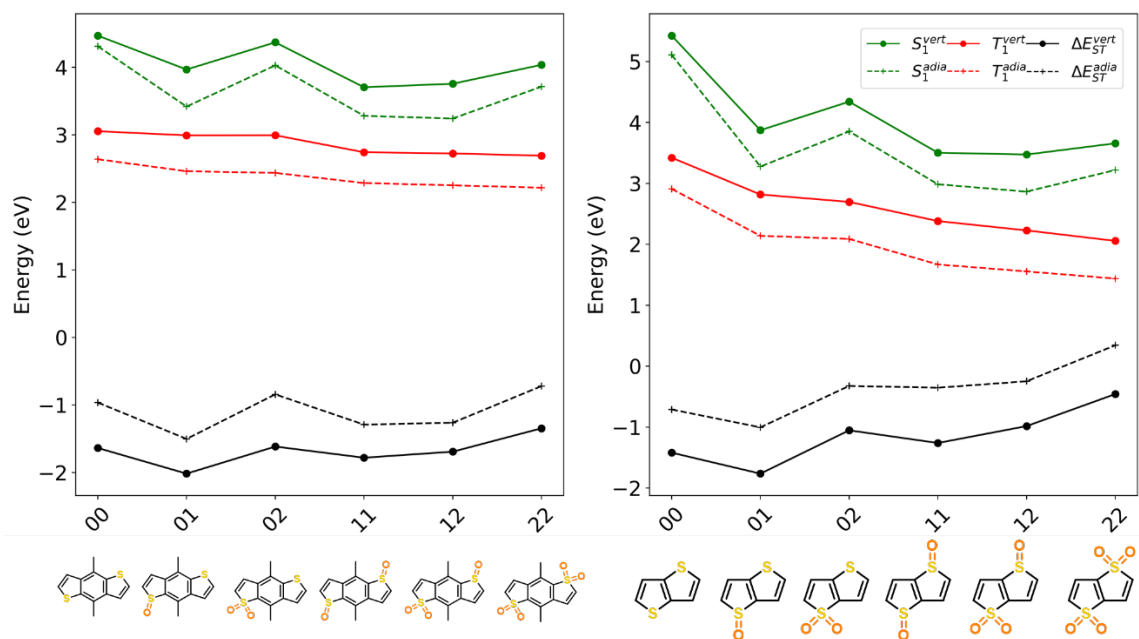
Figure S5: Vertical (solid lines) and adiabatic (dotted lines) singlet excitations (*green*), triplet excitations (*red*), and singlet-triplet splitting energies (*black*) of monomers containing two sulfur heteroatoms (benzo[1,2-b:4,5-b']dithiophene (BDT): *left*, thieno[3,2-b]thiophene: *right*) and their oxidized derivatives.
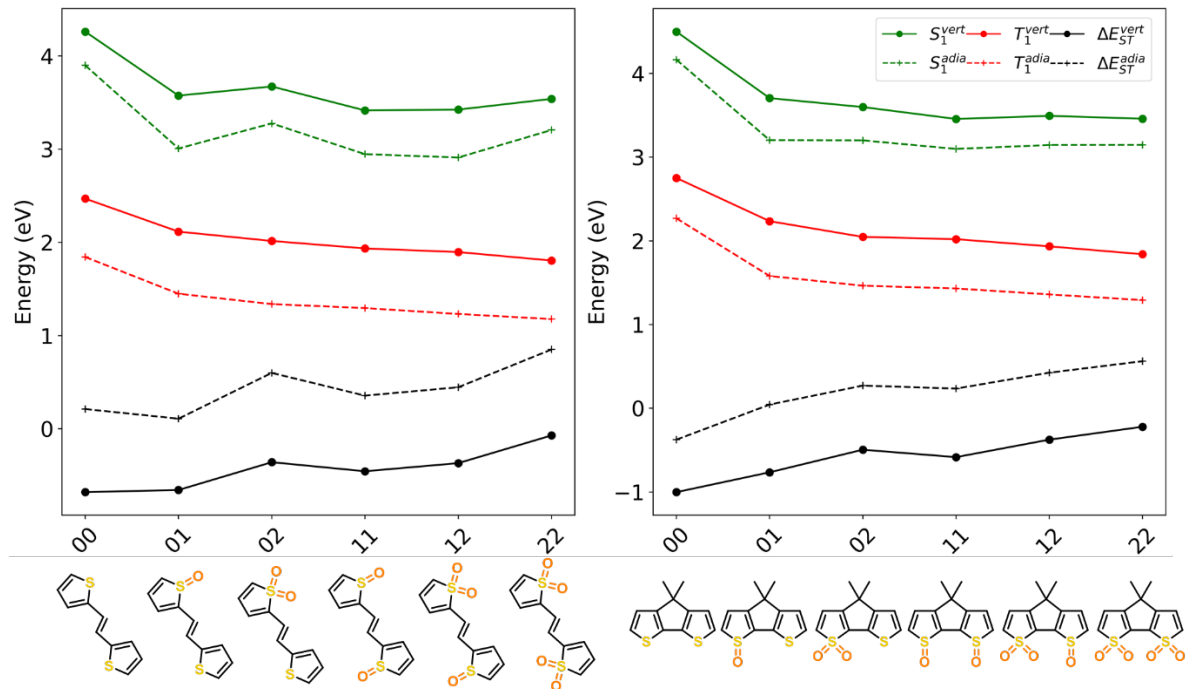

Figure S6: Vertical (solid lines) and adiabatic (dotted lines) singlet excitations (*green*), triplet excitations (*red*), and singlet-triplet splitting energies (*black*) of monomers containing two sulfur heteroatoms (((*E*)-2-(2-(thiophen-2-yl)vinyl)thiophene (TVT): *left*, cyclopenta-[2,1-b:3,4-b′]dithiophene (CPDT): *right*) and their oxidized derivatives.
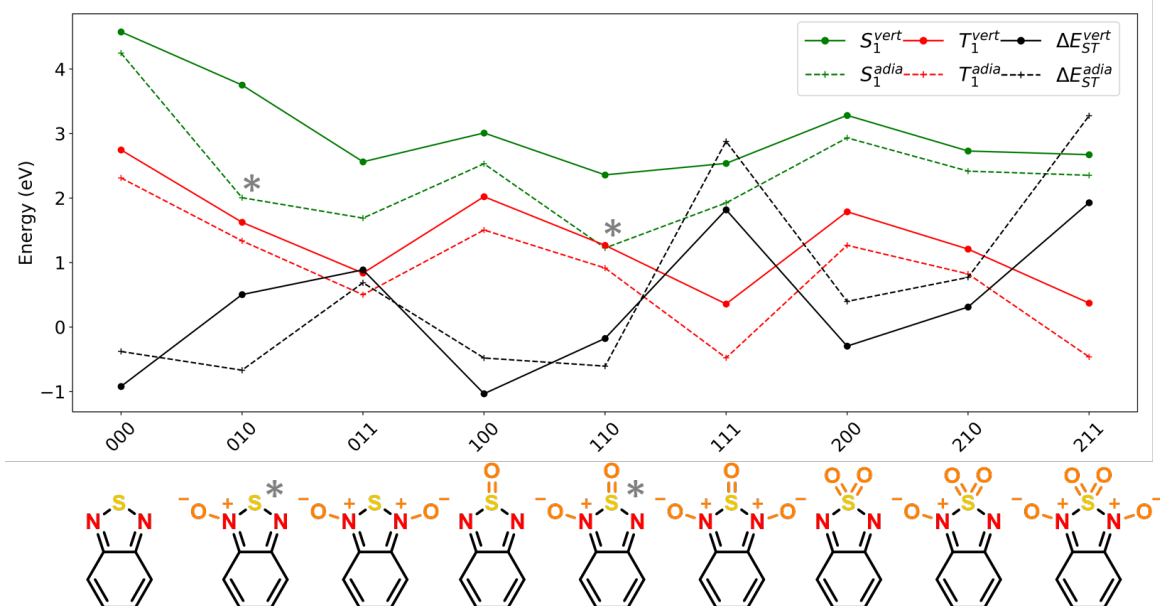
Figure S7: Vertical (solid lines) and adiabatic (dotted lines) singlet excitations (*green*), triplet excitations (*red*), and singlet-triplet splitting energies (*black*) of 2,1,3-benzothiadiazole (BT) and its oxidized derivatives. The compounds marked with an asterisk exhibit ring opening upon relaxation on the S_1 energy surface, leading to uncharacteristically low S_1^{adia} (and consequently low ΔE_{ST}^{adia}) energies. Two compounds result in T_1^{adia} energies below S_0, indicating that these structures in fact have triplet ground states. This was confirmed by reoptimizing their ground states as triplets.
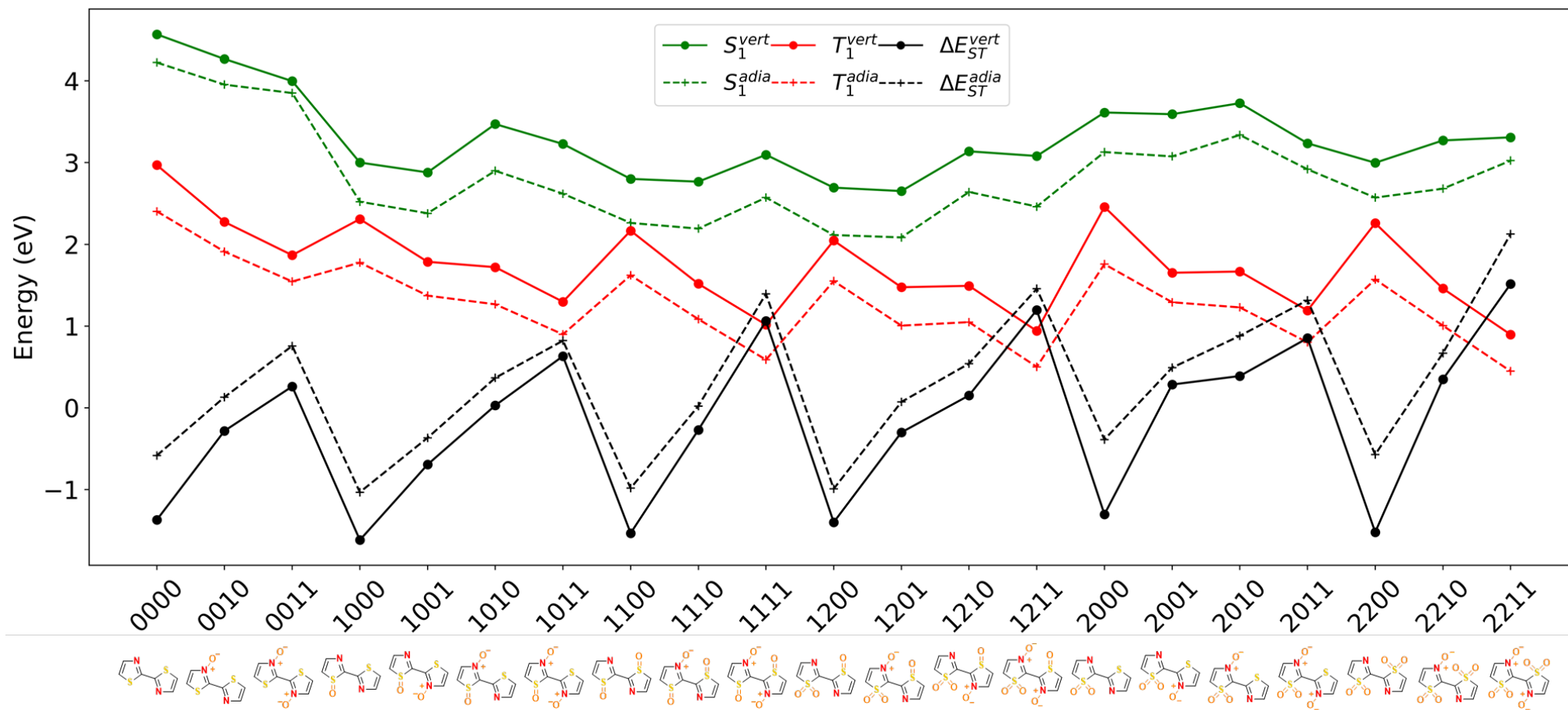
Figure S8: Vertical (solid lines) and adiabatic (dotted lines) singlet excitations (*green*), triplet excitations (*red*), and singlet-triplet splitting energies (*black*) of bithiazole (bTz) and its oxidized derivatives.
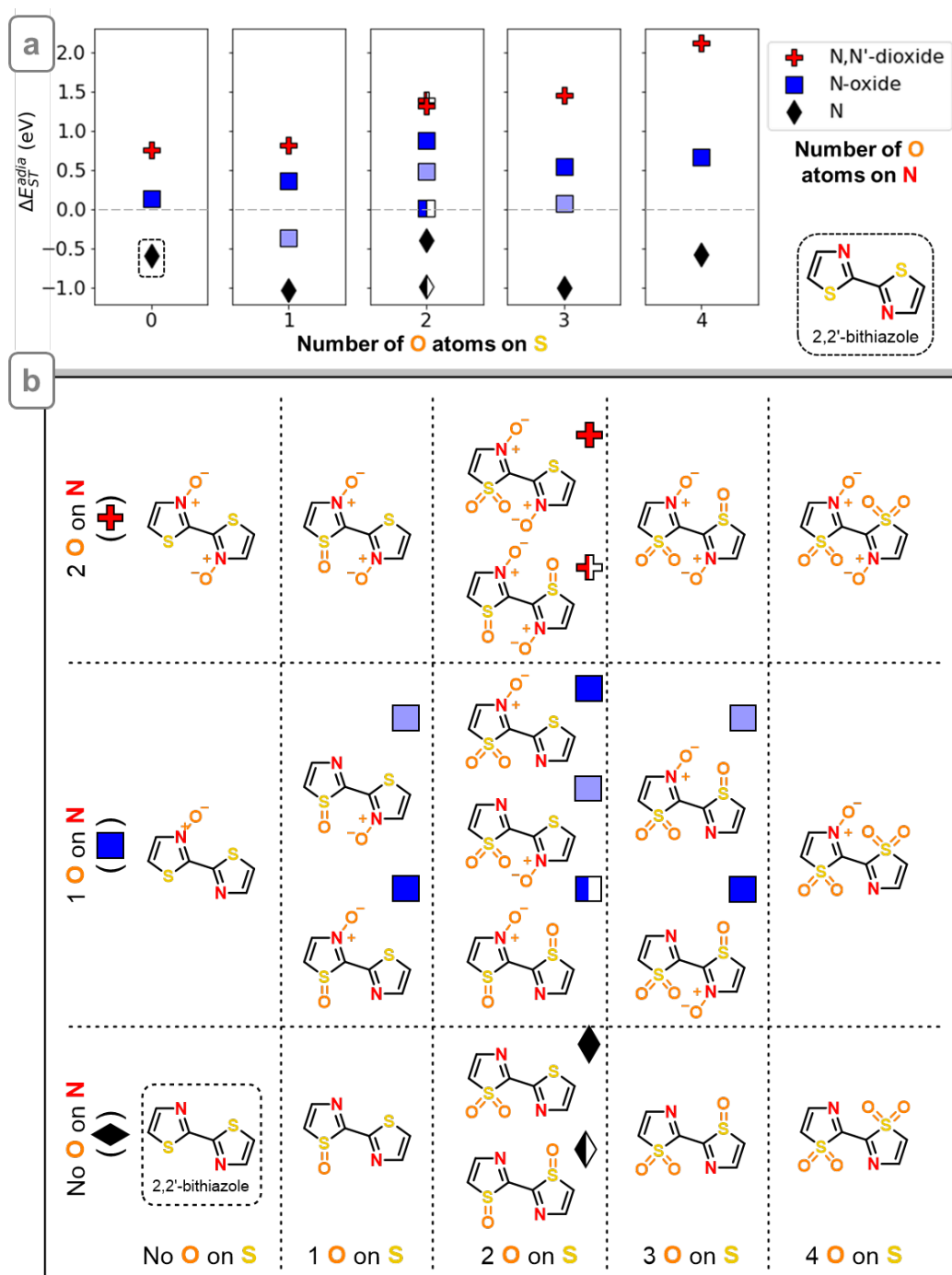
Figure S9: (*a*) Adiabatic singlet-triplet splitting (*y-axis*) for 2,2'-bithiazole (bTz) and its oxidized derivatives, classified by the number of *S*-oxidations (x-axis panels) and the number of *N*-oxidations (label shapes) per compound. In the case of ambiguities in this classification, the corresponding markers are shown explicitly (*i.e.* half-filled and filled markers indicate mono-and di-oxidized sulfur atoms, respectively). The corresponding structures are given in (*b*).
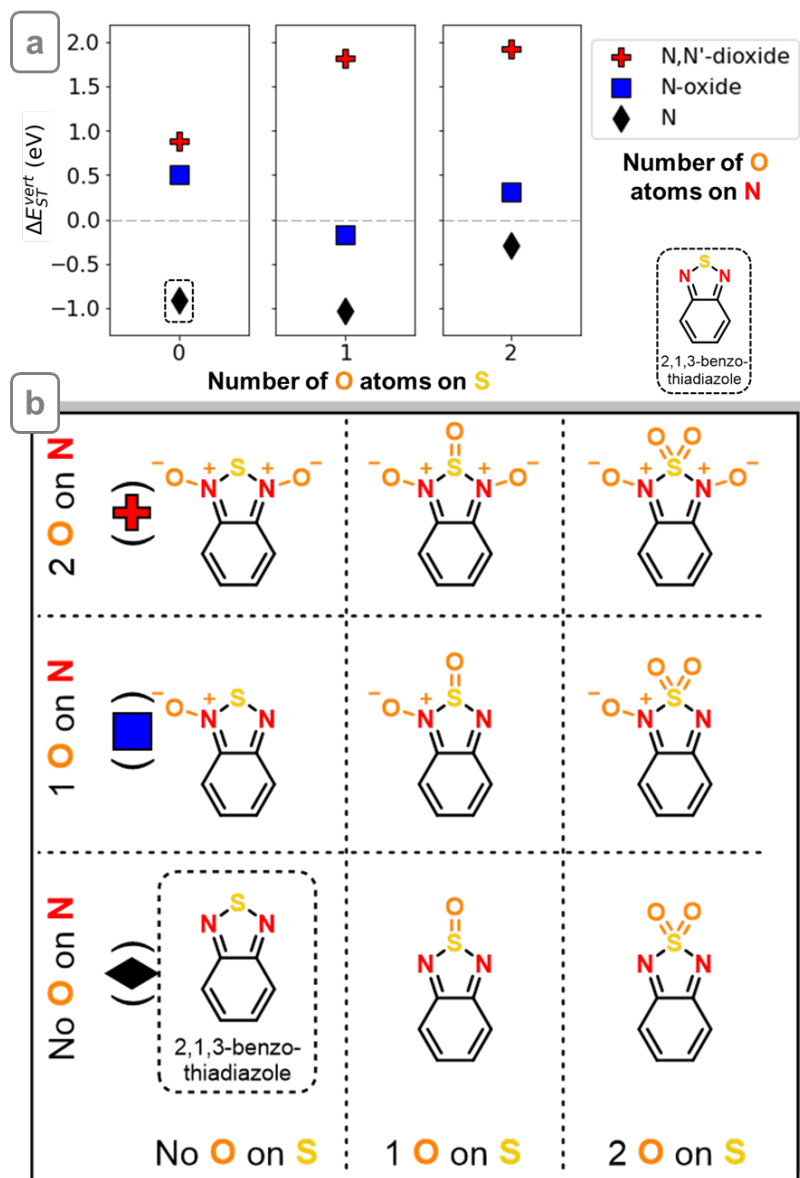
Figure S10: (*a*) Vertical singlet-triplet splitting for 2,1,3-benzothiadiazole (BT) and its oxidized derivatives, classified by the number of S-oxidations (x-axis panels) and the number of *N*-oxidations (label shapes) per compound. The corresponding structures are given in (*b*).
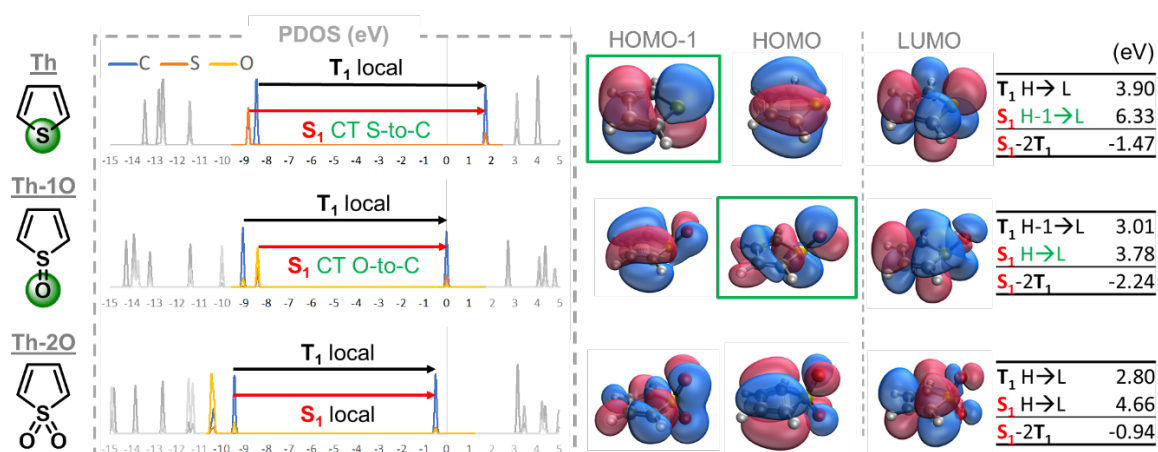
S3. Character of excited states

Figure S11: Projected density of states (PDOS), key molecular orbitals and vertical excitation energies for thiophene (Th) and its two *S*-oxidized derivatives (Th-1O and Th-2O). Transitions between the states most involved in the T_1 and S_1 excitations are marked with black and red arrows, respectively. The molecular orbitals contributing to the charge transfer (CT) character of certain excitations and the atoms on which they are centered are highlighted in green. All energies are given in eV.

Figure S12: Projected density of states (PDOS), key molecular orbitals and vertical excitation energies for thienopyrroledione (TPD) its two *S*-oxidized derivatives (TPD-1O and TPD-2O). Transitions between the states most involved in the T_1 and S_1 excitations are marked with black and red arrows, respectively. The molecular orbitals contributing to the charge transfer (CT) character of certain excitations and the atoms on which they are centered are highlighted in green. All energies are given in eV.
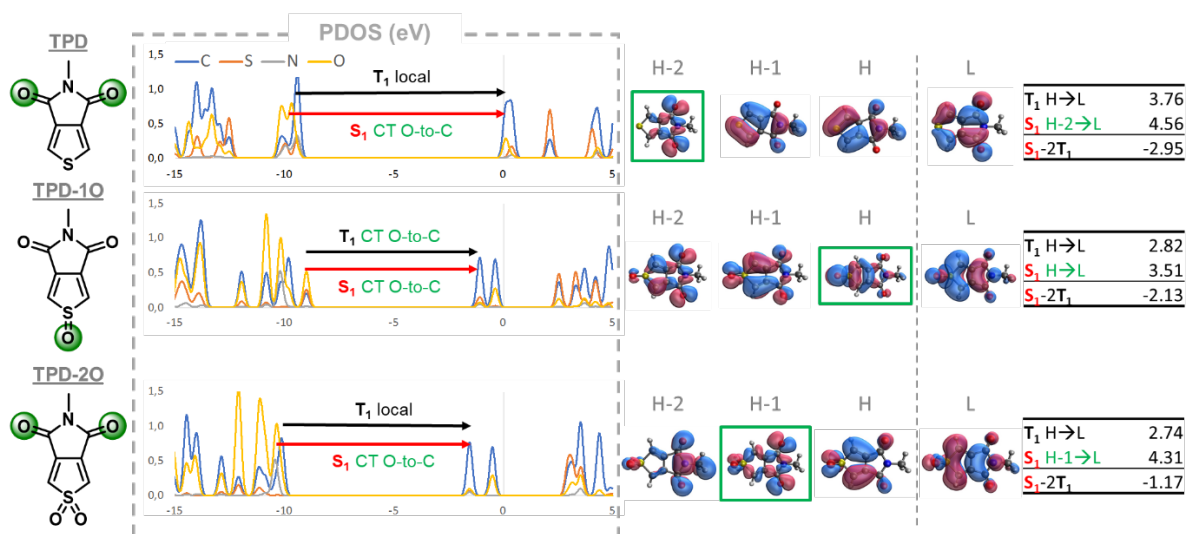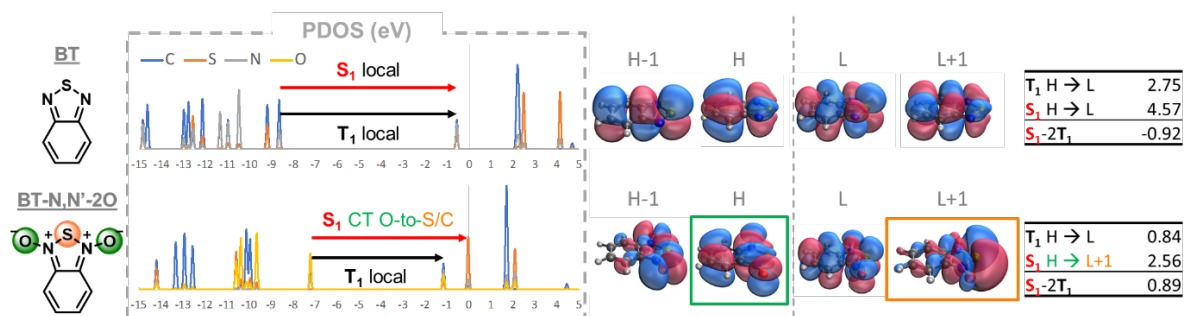
Figure S13: Projected density of states (PDOS), key molecular orbitals and vertical excitation energies for benzothiadiazole (BT) and its *N,N'*-dioxidized derivative (BT-*N,N'*-2O). Transitions between the states most involved in the T_1 and S_1 excitations are marked with black and red arrows, respectively. The molecular orbitals contributing to the charge transfer (CT) character of certain excitations and the atoms on which they are centered are highlighted in green and orange. All energies are given in eV.
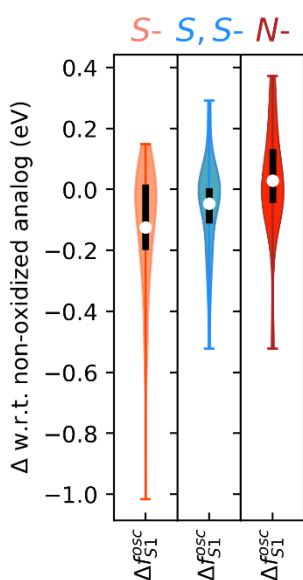

Figure S14: Summary of the change in oscillator strength of the vertical S_1 excitation upon *S*-, *S,S*- and *N*-oxidation for all compounds, showing averages (white points), 1st-3rd quartiles (black bars), and maximal/minimal values (whiskers). Averages ± standard deviations by set are -0.12 ± 0.22, -0.05 ± 0.15, 0.03 ± 0.18.

S4. Nucleus-independent chemical shifts

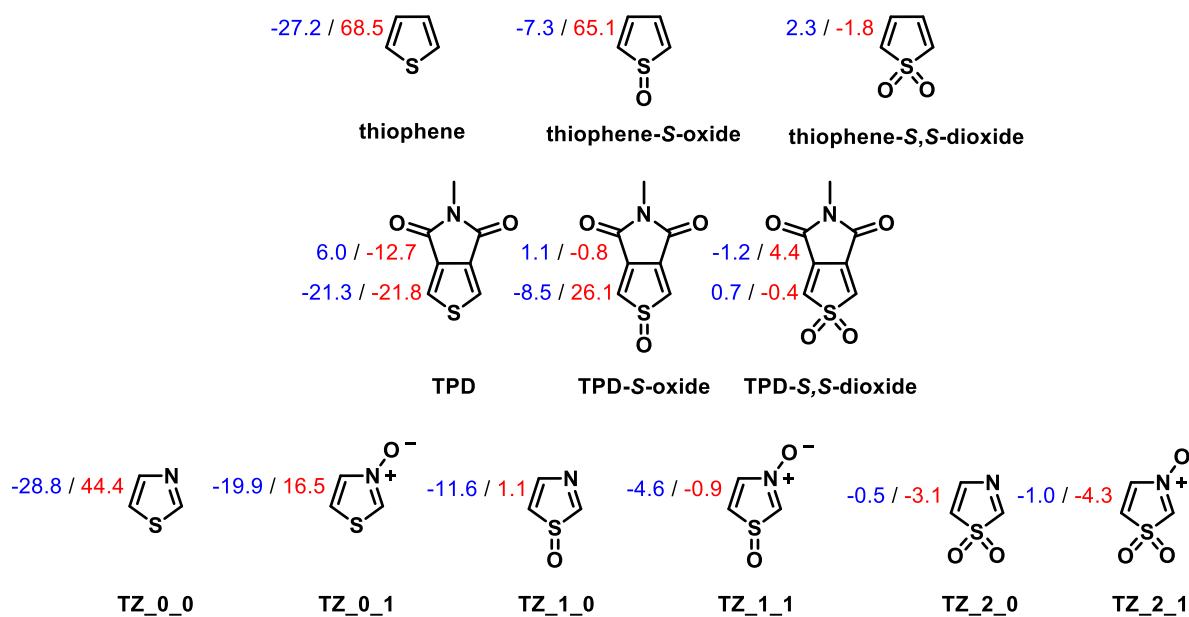**Figure S15**: Out-of-plane component of the magnetic shielding tensor at 1 Ångstrom above each ring (NICS(1)$_{zz}$) in the ground state singlet (*blue*) and triplet (*red*) states at the S$_0$ geometry.
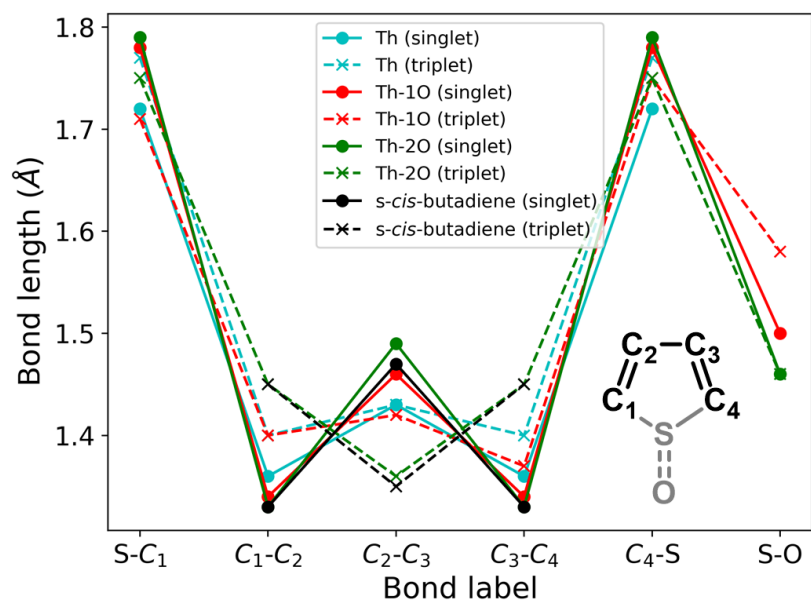
S5. Bond lengths

Figure S16: Bond lengths in non-oxidized (Th), mono-oxidized (Th-1O) and di-oxidized thiophene (Th-2O), in comparison to the equivalent bond lengths of butadiene in the s-*cis* conformation.

S6. Donor-acceptor dimers

Below are summarized the descriptors for intramolecular singlet fission (iSF) in donor-acceptor systems, as proposed in previous work[3,18], for all computed D-A dimers (**Figure S17**). Key properties for five outlying compounds (**A-E**) are reported in **Table S2**, which highlights that all five show promising S_1 charge transfer and local acceptor-based T_1 character, but that **A** and **E** have quite low T_1 energies. Given than the three remaining compounds (**B-D**) contain a *S,S*-dioxidized benzothiadiazole moiety which was not included in previously-reported benchmarking of these descriptors[3], we recomputed the key properties for **B-D** with coupled cluster to second order (CC2) and algebraic diagrammatic construction through second order (ADC(2), **Table S3**). Similar trends between ADC(2) and CC2 and the reported TDA-TDDFT results are observed across all three compounds. The absolute values show the same tendencies as found in the previous benchmarking work: somewhat higher T_1 energies and lower S_1 energies are observed compared to TDA-TDDFT, as well as moderately lower local acceptor character in T_1 and higher S_1 charge transfer. As a result, we note that if we were to conduct ADC(2) or CC2 computations to identify new SF candidates, we would require a different vertical excitation threshold for energy splitting. In other words, given that the thermodynamic cut-off used here ($\Delta E_{ST}^{vert} = S_1^{vert} - 2 * T_1^{vert} \geq -1 \, eV$) is method-dependent, as it was identified empirically from TDA-TDDFT results, it would have to be adjusted for ADC(2)- or CC2-computed excitation energies.

Finally, the energy and character of the higher excited states for the most promising dimer (**B**) are reported in relation to the low-lying states (S_1 and ^{1}TT) invoked in the context of the D-A-based iSF mechanism (**Figure S18**). It is shown that the $S_1 \rightarrow ^1$TT process is slightly exergonic once relaxation of excited state geometry is considered. Given that this process is spin-conserving (internal conversion), and that the ^{1}TT state is the closest in energy to S_1, it is expected that even though the process of population transfer from S_1 to the triplet manifold may be possible (intersystem crossing), the $S_1 \rightarrow ^1$TT transition required for iSF is the most efficient decay pathway.
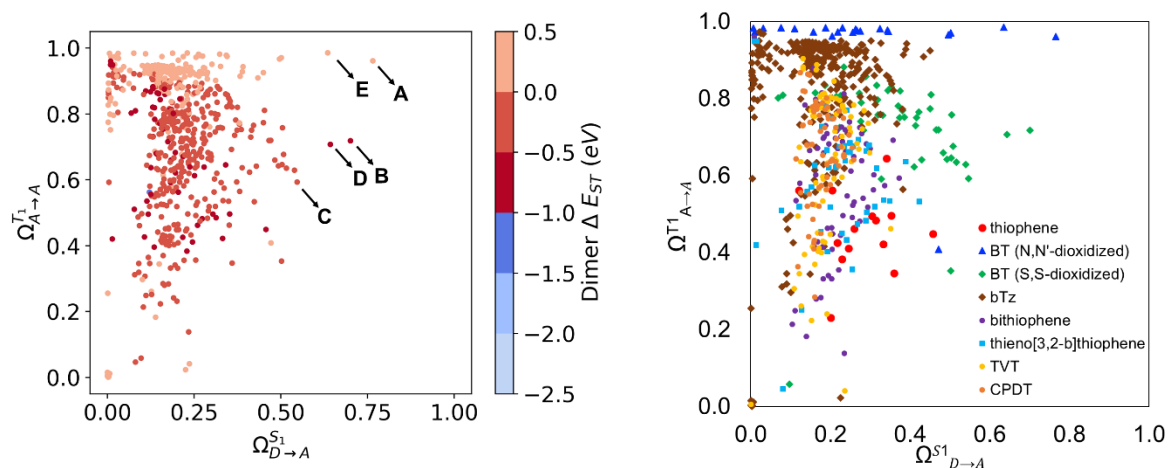

Figure S17: Donor-to-acceptor charge-transfer character of S_1 ($\Omega_{D\rightarrow A}^{S1}$, x-axis) and local acceptor character of T_1 ($\Omega_{A\rightarrow A}^{T1}$, y-axis) in the dimers, colored by the vertical singlet-triplet splitting in the dimer (ΔE_{ST}^{vert}, *left*) and by the nature of the acceptor (*right*). As predicted from monomer energy splitting, all dimers show $\Delta E_{ST}^{vert} \geq$ -1.0 eV. The compound labels on the right distinguish between the benzothiadiazole (BT) acceptors which are oxidized at both nitrogens and may or may not be oxidized at sulfur (such as compounds A and E; blue triangles), and those which are *only* dioxidized at sulfur (such as compounds B, C and D; green diamonds).

Table S2: Vertical excited state properties of a selection of dimers, as labelled in **Figure 2** and **Figure S17**.
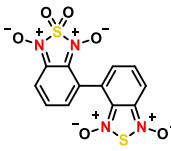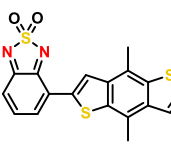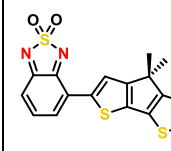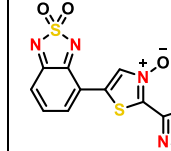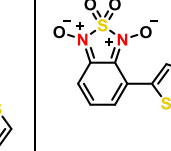
Label	A	B	C	D	E
Structure					
Acceptor	BT_211	BT2_200	BT2_200	BT2_200	BT_211
Donor	BT_011	BDT_00	CPDT_00	bTz_0010	bTz_0011
S_1^{vert} (eV)	2.26	2.41	2.22	2.48	2.47
T_1^{vert} (eV)	0.41	1.47	1.24	1.49	0.37
ΔE_{ST}^{vert} (eV)	1.45	-0.53	-0.26	-0.50	1.73
$\Omega_{D \to A}^{S1}$	0.77	0.70	0.55	0.64	0.64
$\Omega_{A \to A}^{T1}$	0.96	0.72	0.59	0.71	0.99
$f^{osc}(S_1^{vert})$	0.143	0.195	0.319	0.231	0.080
φ_{D-A} (°)	61	30	19	21	66
Index in dataset	ACC2_211_ ACC2_011	ACC2_200_ DON1_00	ACC2_200_ DON9_00	ACC2_200_ ACC5_0010	ACC2_211_ ACC5_0011

Table S3: Benchmarking of key vertical excited state properties of the best dimer candidates, as labelled in **Figure 2** and **Figure S17**. TDA-TDDFT results are shown in grey, followed by coupled cluster to second order (CC2) and algebraic diagrammatic construction through second order (ADC(2)) results.

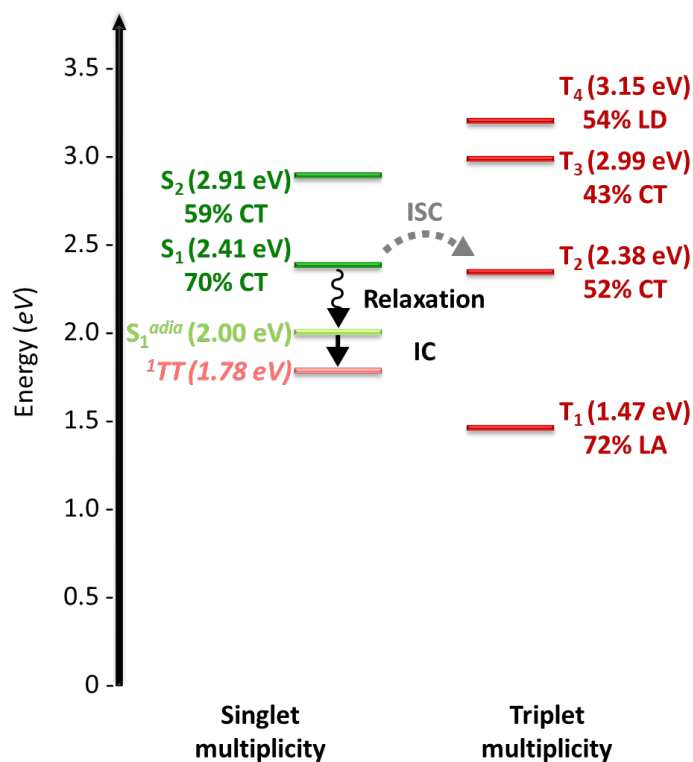|		B	C	D
	Label and structure			
Property	**Method**			
S_1 (eV)	TDA-TDDFT	2.41	2.22	2.48
	CC2	2.07	1.87	1.94
	ADC(2)	1.98	1.80	1.67
T_1 (eV)	TDA-TDDFT	1.47	1.24	1.49
	CC2	1.66	1.40	1.65
	ADC(2)	1.60	1.34	1.50
ΔE_{ST}^{vert} (eV)	TDA-TDDFT	-0.53	-0.26	-0.50
	CC2	-1.25	-0.93	-1.37
	ADC(2)	-1.22	-0.89	-1.33
$\Omega_{D \to A}^{S1}$	TDA-TDDFT	0.70	0.55	0.64
	CC2	0.83	0.68	0.85
	ADC(2)	0.83	0.68	0.86
$\Omega_{A \to A}^{T1}$	TDA-TDDFT	0.72	0.59	0.71
	CC2	0.53	0.45	0.42
	ADC(2)	0.52	0.46	0.24

Figure S18: Energy and largest contributions to the character of higher excited states in the Franck-Condon regime for the best donor-acceptor system presented above (compound **B**). The left-hand column indicates states with singlet multiplicity and the righthand column states with triplet multiplicity. Transitions between the two columns constitute intersystem crossings (ISC), which are less favourable than transitions within one column (internal conversion, IC). The IC pathway required for iSF is marked with a black arrow, and a less likely ISC deactivation channel is marked with a dotted grey arrow. The pale green point indicates the adiabatic S_1 energy and the pink point indicates the approximate energy of the correlated triplet-pair state (^1TT, twice the adiabatic T_1 energy), which retains an overall singlet character. For state character: LA = local acceptor-based character, LD = local donor-based character, CT = donor-to-acceptor charge transfer character.

S7. References

(1)   M. J. Frisch, G. W. T., H. B. Schlegel, G. E. Scuseria, M. A. Robb, J. R. Cheeseman, G. Scalmani, V. Barone, G. A. Petersson, H. Nakatsuji, X. Li, M. Caricato, A. Marenich, J. Bloino, B. G. Janesko, R. Gomperts, B. Mennucci, H. P. Hratchian, J. V. Ortiz, A. F. Izmaylov, J. L. Sonnenberg, D. Williams-Young, F. Ding, F. Lipparini, F. Egidi, J. Goings, B. Peng, A. Petrone, T. Henderson, D. Ranasinghe, V. G. Zakrzewski, J. Gao, N. Rega, G. Zheng, W. Liang, M. Hada, M. Ehara, K. Toyota, R. Fukuda, J. Hasegawa, M. Ishida, T. Nakajima, Y. Honda, O. Kitao, H. Nakai, T. Vreven, K. Throssell, J. A. Montgomery, Jr., J. E. Peralta, F. Ogliaro, M. Bearpark, J. J. Heyd, E. Brothers, K. N. Kudin, V. N. Staroverov, T. Keith, R. Kobayashi, J. Normand, K. Raghavachari, A. Rendell, J. C. Burant, S. S. Iyengar, J. Tomasi, M. Cossi, J. M. Millam, M. Klene, C. Adamo, R. Cammi, J. W. Ochterski, R. L. Martin, K. Morokuma, O. Farkas, J. B. Foresman, and D. J. Fox Gaussian 09, Revision D.01 *Gaussian, Inc., Wallingford CT.* **2016**.

(2)   Peach, M. J.; Tozer, D. J. Overcoming low orbital overlap and triplet instability problems in TDDFT. *J. Phys. Chem. A* **2012**, *116*, 9783-9789.

(3)   Blaskovits, J. T.; Fumanal, M.; Vela, S.; Corminboeuf, C. Designing Singlet Fission Candidates from Donor–Acceptor Copolymers. *Chem. Mater.* **2020**, *32*, 6515-6524.

(4)   Mai, S.; Plasser, F.; Dorn, J.; Fumanal, M.; Daniel, C.; González, L. Quantitative wave function analysis for excited states of transition metal complexes. *Coord. Chem. Rev.* **2018**, *361*, 74-97.

(5)   O'boyle, N. M.; Tenderholt, A. L.; Langner, K. M. Cclib: a library for package-independent computational chemistry algorithms. *J. Comput. Chem.* **2008**, *29*, 839-845.

(6)   Plasser, F.; Lischka, H. Analysis of excitonic and charge transfer interactions from quantum chemical calculations. *J. Chem. Theory Comput.* **2012**, *8*, 2777-2789.

(7)   Plasser, F. TheoDORE: A toolbox for a detailed and automated analysis of electronic excited state computations. *J. Chem. Phys.* **2020**, *152*, 084108.

(8)   Schleyer, P. v. R.; Maerker, C.; Dransfeld, A.; Jiao, H.; van Eikema Hommes, N. J. R. Nucleus-Independent Chemical Shifts: A Simple and Efficient Aromaticity Probe. *J. Am. Chem. Soc.* **1996**, *118*, 6317-6318.

(9)   Lee, C.; Yang, W.; Parr, R. G. Development of the Colle-Salvetti correlation-energy formula into a functional of the electron density. *Phys Rev B* **1988**, *37*, 785-789.

(10)   Becke, A. D. Density-functional thermochemistry. III. The role of exact exchange. *J. Chem. Phys.* **1993**, *98*, 5648-5652.

(11)   Ditchfield, R. Self-consistent perturbation theory of diamagnetism. *Mol. Phys.* **1974**, *27*, 789-807.

(12)   Wolinski, K.; Hinton, J. F.; Pulay, P. Efficient implementation of the gauge-independent atomic orbital method for NMR chemical shift calculations. *J. Am. Chem. Soc.* **1990**, *112*, 8251-8260.

(13)   Schirmer, J. Beyond the random-phase approximation: A new approximation scheme for the polarization propagator. *Phys. Rev. A* **1982**, *26*, 2395.

(14)   Trofimov, A.; Schirmer, J. An efficient polarization propagator approach to valence electron excitation spectra. *J. Phys. B: At. Mol. Opt. Phys.* **1995**, *28*, 2299.

(15)   Ahlrichs, R.; Bär, M.; Häser, M.; Horn, H.; Kölmel, C. Electronic structure calculations on workstation computers: The program system turbomole. *Chem. Phys. Lett.* **1989**, *162*, 165-169.

(16)   Lyakh, D. I.; Musiał, M.; Lotrich, V. F.; Bartlett, R. J. Multireference Nature of Chemistry: The Coupled-Cluster View. *Chem. Rev.* **2012**, *112*, 182-243.

(17)   Christiansen, O.; Koch, H.; Jørgensen, P. The second-order approximate coupled cluster singles and doubles model CC2. *Chem. Phys. Lett.* **1995**, *243*, 409-418.

(18)   Blaskovits, J. T.; Fumanal, M.; Vela, S.; Fabregat, R.; Corminboeuf, C. Identifying the Trade-off between Intramolecular Singlet Fission Requirements in Donor–Acceptor Copolymers. *Chem. Mater.* **2021**, *33*, 2567-2575.